Identification of Vortical Flow Pattern inside PWR Fuel Assembly

Gong Hee Lee

Korea Institute of Nuclear Safety, 62 Gwahak-ro, Yuseong-gu, Daejeon, 34142, Republic of Korea, ghlee@kins.re.kr
Nuclear and Radiation Safety Department, University of Science and Technology, Daejeon 34133, Korea

Ae Ju Cheong

Korea Institute of Nuclear Safety, 62 Gwahak-ro, Yuseong-gu, Daejeon, 34142, Republic of Korea, k495caj@kins.re.kr

Abstract *- In this study, in order to examine the vortical flow structure inside fuel assembly with mixing vanes, simulations were conducted with the commercial CFD software, ANSYS CFX R.14. The predicted results were compared with the measured data from the MATiS-H test facility. Through these comparisons, it was concluded that although there were locally differences between the prediction and the measurement, ANSYS CFX R.14 could qualitatively predict the time averaged vortical flow inside fuel assembly with mixing vanes. Additionally either absolute helicity or Q-criterion could efficiently identify vortex core region in the subchannel. Vortical flow distributions inside fuel assembly were significantly different, depending on the arrangement pattern of the mixing vane.*

I. INTRODUCTION

In a PWR (Pressurized Water Reactor), the appropriate heat removal from the surface of fuel rod bundle is important for thermal margins and safety. A spacer grid that supports the fuel rods in a fuel assembly is equipped with mixing vanes that play a role in improving the heat transfer from the hot surfaces of the fuel rods to the coolant flow as the turbulence-enhancing devices.

As showin in Fig. 1, flow patterns generated by a spacer grid with mixing vanes generally consist of both the swirl flow inside subchannel and the cross flow at the fuel rod gaps. The swirl flow improves the heat removal at the fuel rod surface by mixing the hot water near the fuel rod surface with the relatively cold water at the subchannel center, while the cross flow contributes to mitigating the hot peaking of subchannels by exchanging the enthalpy between subchannels[1]. Therefore, the geometrical shape and arrangement of the mixing vane are important factors that determine the performance of the mixing vane.

Because a spacer grid may cause rigorous mixing as well as greatly increased local turbulence levels inside the sub-channel, prediction of sub-channel flows, even in isothermal condition, is very difficult. In general, sub-channel analysis codes such as COBRA or VIPRE have been used to predict the flow and enthalpy distributions within fuel assemblies. However, these sub-channel codes rely on geometrically dependent mixing factors and empirical correlations to close the governing equations. The advantage of a CFD (Computational Fluid Dynamics) software for sub-channel flow predictions is that it does not rely to the same extent on these empiricisms. Therefore, CFD results have the potential for wider applicability to capture the essential features of the turbulent structures downstream of the spacer grid.

In this study, in order to examine the vortical flow structure inside fuel assembly with mixing vanes, simulations were conducted with the commercial CFD software, ANSYS CFX R.14[2]. As shown in Fig. 2, two different types of spacer grids, i.e. split-type and swirl-type, were used. The predicted results were compared with the measured data from the MATiS-H (Measurement and Analysis of Turbulent Mixing in Sub-channels-Horizontal) test facility.

Fig. 1. Flow patterns inside fuel assembly (split-type spacer grid).

(a) split-type[3]   (b) swirl-type[4]
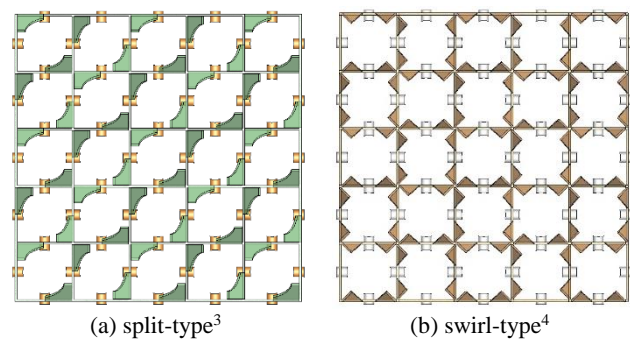
Fig. 2. Spacer grid with mixing vanes (upstream view).

II. ANALYSIS MODEL

MATiS-H test facility[5], installed in the KAERI (Korea Atomic Energy Research Institute), was used to perform hydraulic tests in a rod bundle array under the unheated conditions. The main body of the horizontal test section comprises a 4.67 m-long square duct of inner dimensions 0.17×0.17 m, containing a 3.863 m-long 5×5 rod bundle array. Outer diameter of a fuel rod, rod-to-rod pitch (P), and rod-to-wall pitch were 25.4 mm, 33.12 mm, and 18.75 mm, respectively. The hydraulic diameter (D_h) of the flow cross-section was 24.27 mm. Both 'split-type' and 'swirl-type' spacer grid were installed in the rod bundle for enhancing the lateral turbulent mixing in the sub-channels.

Detailed measurements of velocity components in sub-channels have been obtained using a two-component LDA (Laser Doppler Anemometry) system at four different axial locations (Z = 0.5, 1.0, 4.0 and 10 D_h) from the downstream edge of the mixing vane tip, as shown in Fig. 3. Turbulence intensities and vortices in the sub-channels were then evaluated from the measured velocity components. The mean values and their uncertainties of test conditions are summarized in Table I.

(a) U, V velocity component   (b) W velocity component

(c) downstream locations : axial direction
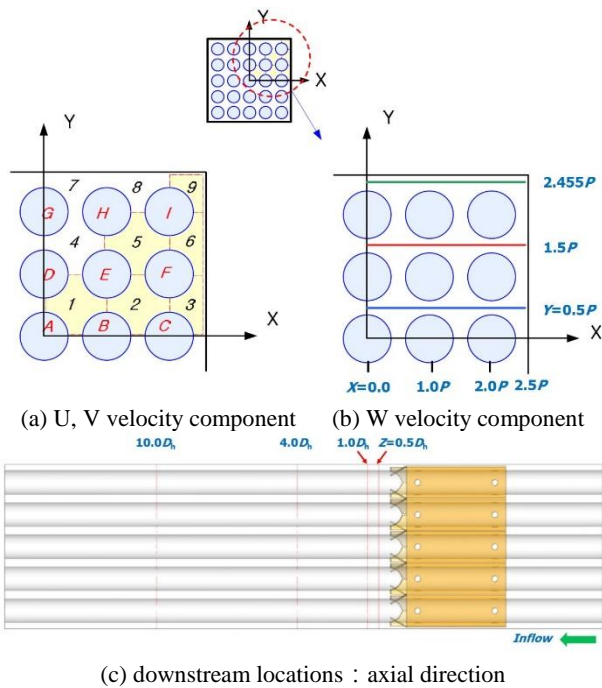
Fig. 3. LDA measurement region[5].

Table I. Test conditions[5]

Parameters	Unit	Mean value	Uncertainty (%)
Mass flow rate	kg/s	24.2	0.29
Temperature	℃	35	2.90
Pressure	kPa	156.9	0.39
Bulk velocity	m/s	1.5	0.37
Reynolds number	-	50,250	2.01

III. NUMERICAL MODELING

The flow inside the fuel assembly was assumed to be unsteady, incompressible, isothermal and turbulent. A high resolution scheme for the convection-terms-of-momentum and -turbulence equations was used. 2nd Order Backward Euler scheme was used for the transient term. A time step of 0.001sec was used with the maximum 10 iterations per time step. Total simulation time was 3sec. The solution was considered 'converged' when the residuals of the variables were below 10^{-5} at each time step. Simulation was conducted with the commercial CFD software, ANSYS CFX R.14[2].

The SSG (Speziale, Sarkar and Gatski) Reynolds stress model was used to simulate the turbulent flow inside fuel assembly. This model may show superior predictive performance compared to eddy-viscosity models in flows with strong streamline curvature, secondary flow, swirl flow and flows with sudden changes in the mean strain rate by solving directly the transport equations for the individual components of the Reynolds stress tensor and the dissipation rate. More detailed descriptions of the SSG Reynolds stress model can be found in the ANSYS CFX-solver modeling guide[2].
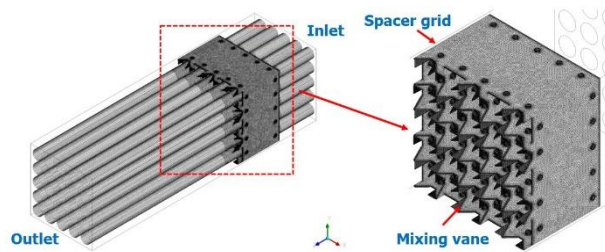
Fig. 4. Grid system for swirl-type spacer grid[4].

Fig. 4 shows the grid system for the computational domain that had the same size as the test facility. A hybrid mesh, made up of tetrahedrons, wedges, pyramids and hexahedrons, was generated to prevent the oversimplification of the geometry, and to have more efficient mesh distribution. Prism layers were used to get higher resolution in the near-wall region. Detailed information for grid system was summarized in Table II.

Table II. Grid information

Parameters	Split-type	Swirl-type
Total elements	$1.77×10^7$	$1.61×10^7$
Max. y+	29.1	27.3

Fully-developed cross sectional profiles of velocity components, obtained from corresponding precursor simulation on Z-periodic (primary flow direction) thin rod bundle, were used as an inlet boundary condition. The 'average pressure over the whole outlet' option; with a relative pressure of 0 Pa, was used as an outlet boundary condition. A no-slip condition was applied at the solid wall.

To model the flow in the near-wall region, the scalable wall function method was applied.

IV. RESULTS AND DISCUSSIONS

1. General Flow Pattern and Validation with Test Data

A. Time Averaged Velocity Profile

Fig. 5 ~ Fig. 7 show the time averaged horizontal, vertical and axial velocity profile respectively at $Y = 0.5P$ and at four different axial locations (Z = 0.5, 1.0, 4.0 and 10 D_h) from the downstream edge of the mixing vane tip, as shown in Fig. 3.

Horizontal velocity component (U/W_{bulk})

For the split-type spacer grid, velocity profile of the wave form with the negative and positive peak values were observed near $X/P = 1.0$ and 2.0 due to the cross flow moving to the adjacent subchannel in the vicinity of the mixing vane tip ($Z = 0.5\ D_h$, $1.0\ D_h$). As the flow moved downstream, the peak velocity value disappeared and changed to the flat velocity profile.

In the case of the swirl-type spacer grid, the cross flow moving to the adjacent subchannel by the mixing vanes hardly generated and therefore the velocity shape of the flow through the mixing vanes showed an almost flat shape without shape change even in the downstream.

Except that the predicted results over-predicted the negative horizontal velocity in comparison with the measurements for the split-type spacer grid, the calculated velocity profiles were generally consistent with the measurements.

(a) $Z = 0.5\ D_h$ (b) $Z = 1.0\ D_h$

(c) $Z = 4.0\ D_h$ (d) $Z = 10.0 D_h$
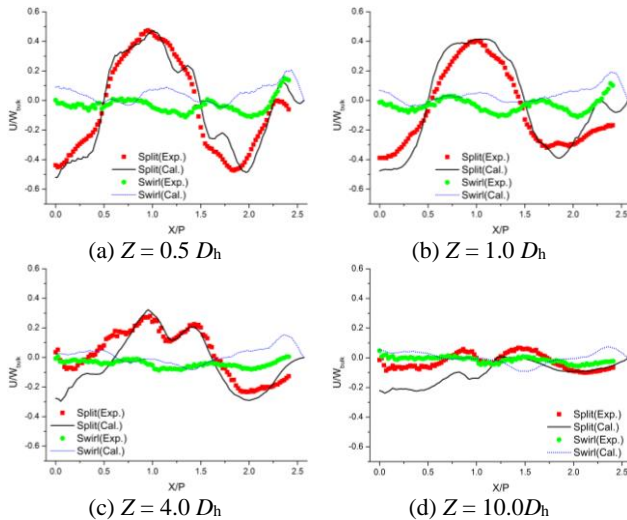
Fig. 5. Time averaged horizontal velocity (U/W_{bulk}) profile at Y=0.5P.

Vertical velocity component (V/W_{bulk})

The velocity profile of the wave form with negative and positive peak values were generated due to the swirl flow inside suhchannels. The peak velocity value gradually decreased as the flow moved downstream.

Based on the interface ($X/P = 1.0$) where two adjacent subchannels border, velocity profile was nearly symmetrical pattern for the swirl-type spacer grid. On the other hand, velocity profile was asymmetric for the split-type spacer grid. The reason may be that in the case of the split-type spacer grid, the vortex shape was elliptical inside subchannels, while it was almost circular for the swirl-type spacer grid, as shown in Fig. 10 and Fig. 11.

Except that the predicted V/W_{bulk} had a relatively large negative and positive peak value compared to the measurements, the calculated velocity profiles were generally consistent with the measurements.

(a) $Z = 0.5\ D_h$ (b) $Z = 1.0\ D_h$

(c) $Z = 4.0\ D_h$ (d) $Z = 10.0 D_h$
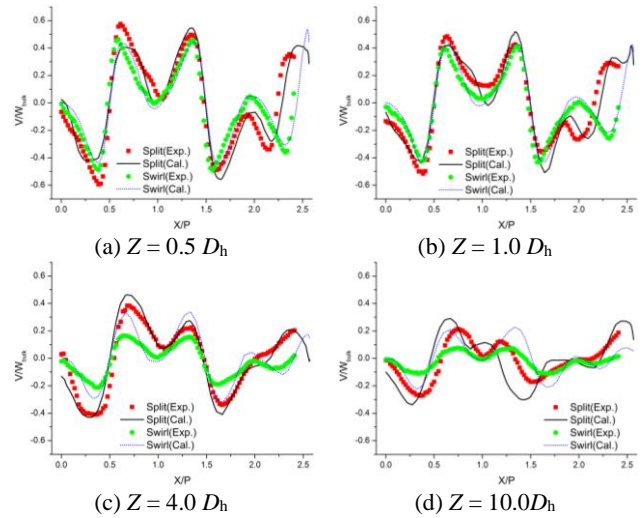
Fig. 6. Time averaged vertical velocity (V/W_{bulk}) profile at Y=0.5P.

Axial velocity component (W/W_{bulk})

As the flow moved downstream, the profile of time-averaged axial velocity component became gradually flat. The reason may be that the defect of W/W_{bulk} caused by mixing vanes disappeared.

The predicted W/W_{bulk} had a relatively large negative and positive peak value compared to the measurements. The velocity profile also changed more frequently.

Quantitative comparisons

The predicted results with the measured data obtained from the MATiS-H test facility were compared by using the following equation:

$$Score = \sum_{i=1,N} \left| Vel_{comp,i} - Vel_{\exp,i} \right|$$

where N is total numbers of test data, $Vel_{comp,i}$ and $Vel_{exp,i}$ are the calculated and measured velocity components at the corresponding measurement positions.

(a) $Z = 0.5\ D_h$ (b) $Z = 1.0\ D_h$

(c) $Z = 4.0\ D_h$ (d) $Z = 10.0 D_h$
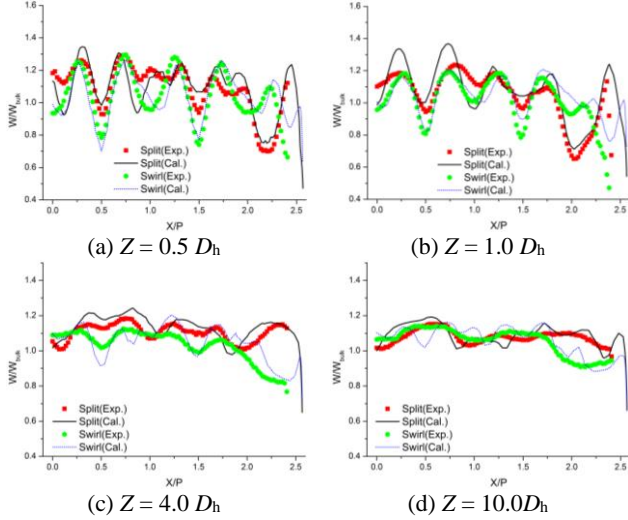
Fig. 7. Time averaged axial velocity (W/W_{bulk}) profile at $Y=0.5P$.

Total score of 91.55 for the split-type spacer grid and 74.083 for the swirl-type spacer grid were in the range of 53.04~151.31 and 46.03~165.12 respectively, obtained from the OECD/NEA benchmark participants. Therefore, the numerical modeling used in this study is valid, and the calculated time averaged velocity results are expected to be reliable.

B. Mixing Factor

The cross flow passing through the gap between the fuel rods (see Fig. 1) is influenced by the arrangement pattern of the mixing vanes attached to the spacer grid, and the mixing factor indicating the strength of the cross flow can be defined as follows:

$$F_{mixing} = \frac{1}{s}\int \frac{\left|V_{gap}\right|}{W_{bulk}}ds$$

where $\left|V_{gap}\right|$ is the cross flow in a gap between fuel rods, s. The mixing factor is the average of the values calculated for the four gaps per a subchannel.

Fig. 8 shows the change in the magnitude of the mixing factor in the downstream direction from the mixing vane tip with respect to some of subchannels (SC#1, 2, 5) in which either split-type or swirl-type spacer grid are arranged in balance.

Split-type spacer grid

Inside subchannels, the strong cross flow moving to the adjacent subchannel was generated. Therefore, the mixing factor showed the equivalent magnitude in comparison with the swirl factor in Fig. 9.

(a) split-type   (b) swirl-type
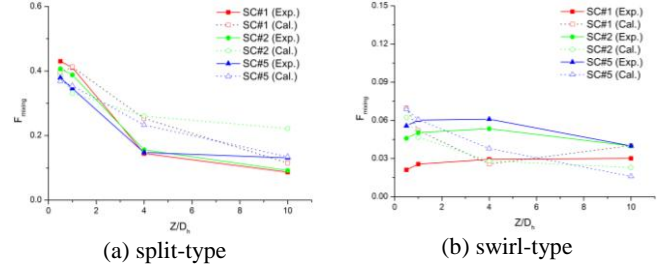
Fig. 8. Mixing factor for the selected subchannels.

The predicted magnitude of the mixing factor decreased drastically to $Z = 4.0\ D_h$, similar to the measurements on the whole, and after which the decay rate was reduced.

Swirl-type spacer grid

Inside subchannels, the cross flow moving to the adjacent subchannel was rarely generated and the swirling flow predominated. Therefore, the mixing factor was relatively small compared to the swirl factor in Fig. 9.

(a) split-type   (b) swirl-type
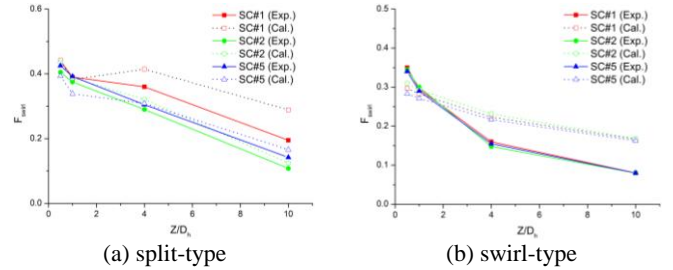
Fig. 9. Swirl factor for the selected subchannels.

In the case of measurement, the magnitude of the mixing factor measured at the subchannel number 2 and 5 (SC#2, 5) was slightly decreased at $Z = 10.0\ D_h$ after maintaining or slightly increasing to $Z = 4.0\ D_h$. The magnitude of the mixing factor measured at the subchannel number 1 (SC#1) did not decrease until $Z = 10.0\ D_h$.

On the other hand, in the case of the calculation, the magnitude of the mixing factor predicted at the subchannel number 2 and 5 (SC#2, 5) decreased as the flow moved downstream. The magnitude of the mixing factor predicted at the subchannel number 1 (SC#1) decreased until $Z = 4.0\ D_h$ and then slightly increased at $Z = 10.0\ D_h$. The slight difference between the measured and the predicted mixing factor may be resulted from the difference in the measured and the calculated local velocities, as shown in Fig. 5 and Fig. 6.

C. Swirl Factor

Swirl factor represents the strength of the swirl flow in the center of subchannel and is defined as follows:

$$F_{swirl} = \frac{1}{l}\int \frac{\left|V_{diag}\right|}{W_{bulk}}dl$$

where l is the diagonal line between fuel rods, $\left|V_{diag}\right|$ is the velocity which is perpendicular to l. Therefore, the swirl factor is the average of the values calculated for two diagonal lines per a subchannel.

Fig. 9 shows the change in the magnitude of the swirl factor in the downstream direction from the mixing vane tip with respect to some of subchannels (SC#1, 2, 5) in which either split-type or swirl-type mixing vanes are arranged in balance.

Split-type spacer grid

In the case of measurement, as the flow moved downstream, the influence of the mixing vane on the flow gradually disappeared, and the magnitude of the swirl factor tended to decrease in the corresponding subchannels.

On the other hand, in the case of the calculation, the magnitude of the mixing factor predicted at the subchannel number 2 and 5 (SC#2, 5) decreased as the flow moved downstream, similar to the measurements. The magnitude of the mixing factor predicted at the subchannel number 1 (SC#1) decreased until $Z = 1.0\ D_h$ and then increased at $Z = 4.0\ D_h$ and finally decreased once again in further downstream. Although the time averaged velocity vector measured at $Z = 4.0\ D_h$ was not open in the literature and therefore direct comparisons with the calculated results were not possible, the tendency difference between some of the swirl factor measurements and the predicted results may be resulted from the difference in measured and predicted local velocities, as shown in Fig. 5 and Fig. 6.

Swirl-type spacer grid

As the flow moved downstream, the magnitude of the swirl factor tended to decrease in both the test and calculation results. Generally, it is well-known that in the fuel assemblies, the local critical heat flux tends to decrease in the form of exponential function as the distance from the mixing vane tip increases in the downstream direction. Since the swirl flow enhances the convective heat transfer, the decrease in the swirl factor is considered to be related to the decrease in the local critical heat flux. Therefore, the decrease tendency in the magnitude of the swirl flow is expected to be similar to Fig. 9. However, due to differences in measured and calculated local velocities, the decay rate of the swirl factor measured from the mixing vane tip to the downstream direction $Z = 4.0\ D_h$ was larger than the calculated value.

2. Identification of Vortical Flow Pattern

A. Time Averaged Axial Vorticity

Time averaged axial vorticity ω_z can be defined by using the measured horizontal and vertical mean velocity components as follows:

$$\omega_z = \left(\frac{\partial V}{\partial x} - \frac{\partial U}{\partial y} \right)$$

Because the vorticity is equal to twice the rotation of the fluid, it can be used directly to identify vortices. However, a problem associated with this method is that vorticity cannot distinguish between swirling motions and shearing motions.

Fig. 10 and Fig. 11 show the time averaged axial vorticity contour in the sub-channels at two different axial locations, $Z = 1.0\ D_h$ and $10.0\ D_h$, from the downstream edge of the mixing vane tip.

For split-type mixing vanes, the predicted axial vorticity at $Z = 1.0\ D_h$ showed that the positive peak magnitude region in the subchannel #5 was more tilted to the horizontal direction in comparison with the measurement (see Fig. 10(a)). As the flow was going downstream, the vorticity magnitude was gradually decayed because the strength of swirl flow due to the effect of mixing vane became weak. Additionally, at a certain subchannels (#2, #5), the regions with peak negative and positive vorticity magnitude moved from the center of subchannels to the fuel rod wall region due to the effect of crossflow passing through the gaps between fuel rods (see Fig. 10(b)).

In case of swirl-type mixing vanes, the predicted axial vorticity at $Z = 1.0\ D_h$ showed nearly circular shape in the subchannel #1, #2, #4 and #5 (see Fig. 11(a)). As the flow was going downstream, the vorticity magnitude was gradually decayed. This result was similar to split-type mixing vanes. However, crossflow passing through the gaps between fuel rods was so small that vortex core was overall maintained at the centers of subchannels (see Fig. 11(b)).

(a) $Z = 1.0\ D_h$

(b) $Z = 10.0\ D_h$
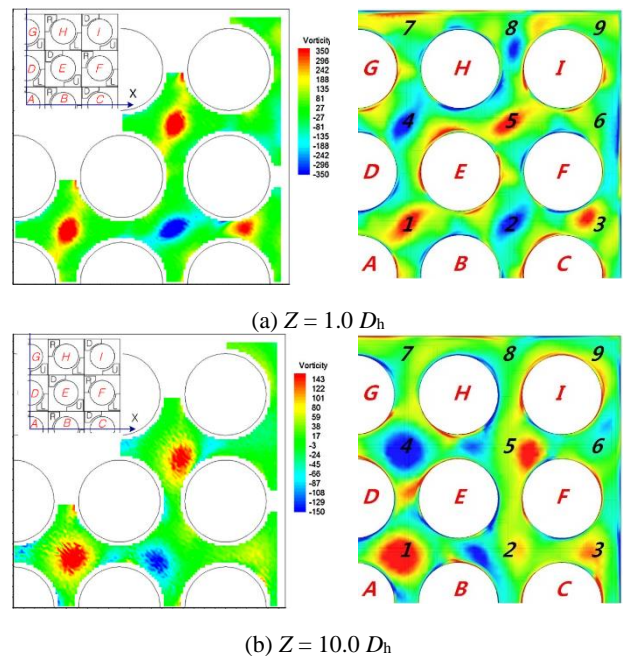
Fig. 10. Time averaged axial vorticity contour – split-type spacer grid (left; experiment, right; calculation).

(a) $Z = 1.0 \, D_h$

(b) $Z = 10.0 \, D_h$
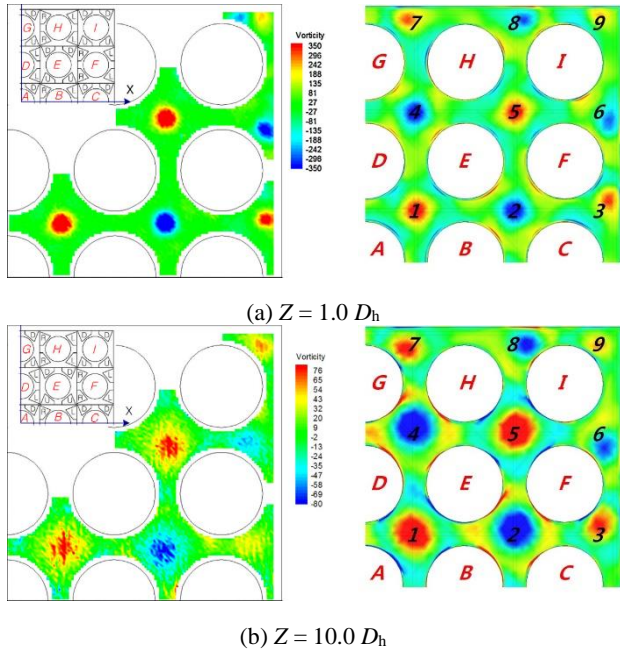
Fig. 11. Time averaged axial vorticity contour – swirl-type spacer grid (left; experiment, right; calculation).

(a) split-type

(b) swirl-type
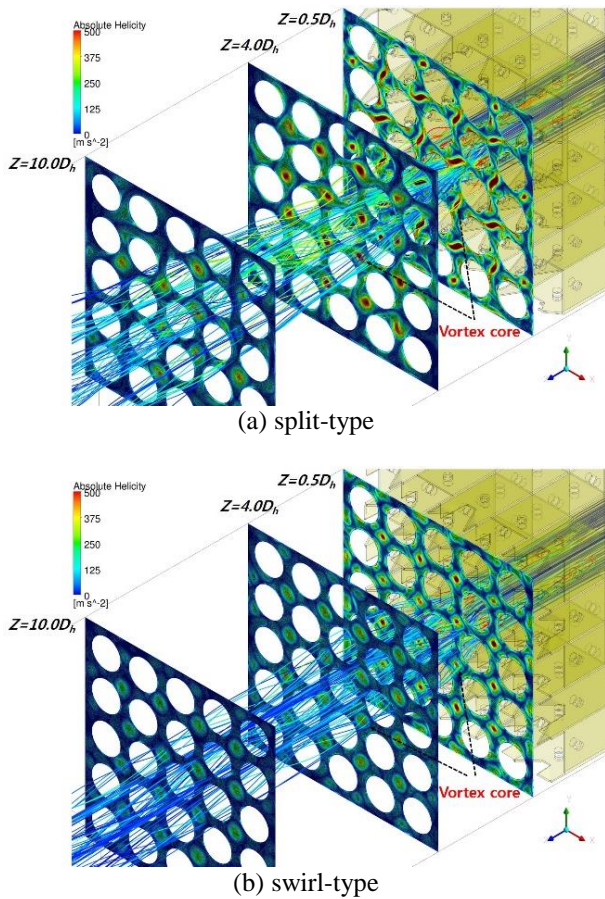
Fig. 12. Streamlines and absolute helicity contour.

B. Absolute Helicity

Absolute helicity H is one of methods to identify the vortex core regions and is defined as the absolute value of the dot product of velocity vector and vorticity vector as follow:

$$H = \left| V_i \cdot \omega_i \right| \qquad i = 1,2,3$$

Fig. 12 shows the streamlines and absolute helicity distribution inside subchannels. Regions with peak magnitudes for absolute helicity represented vortex core and was nearly identical to those with both negative and positive peak magnitude for axial vorticity as shown in Fig. 10 and Fig. 11. Additionally streamline to penetrate such region showed helical shapes.

C. Q Criterion

Q is scalar property and is defined as follow:

$$Q = \frac{1}{2}\left(\overline{\Omega}_{ij}\overline{\Omega}_{ij} - \overline{S}_{ij}\overline{S}_{ij} \right)$$

where $\overline{\Omega}_{ij}$ and $\overline{S}_{ij}$ are time averaged vorticity tensor and strain rate tensor. Therefore Q represents the local balance between vorticity magnitude and strain rate, defining vortices as areas where the vorticity magnitude is greater than that of strain rate.

Fig. 13 shows the center vortices in the subchannel, as identified by the Q criterion ($Q > 0$). As the flow was going downstream, loci of some center vortices for the split-type spacer grid moved from the center of sub-channels (see Fig. 13(a)). On the contrary to this, loci of center vortices for swirl-type spacer grid were maintained at the centers of subchannels (see Fig. 13(b)).

(a) split-type

(b) swirl-type
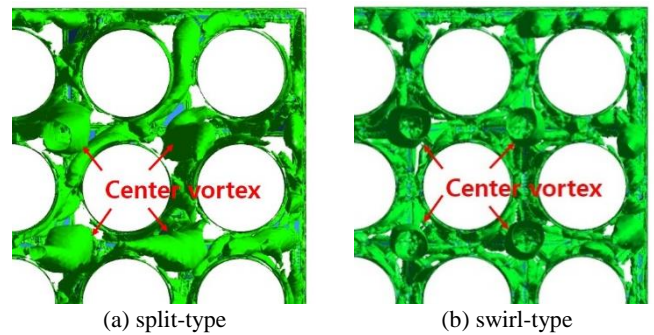
Fig. 13. Center vortices in the subchannel identified by the Q criterion (upstream view).

V. CONCLUSIONS

In this study, in order to examine the vortical flow structure inside fuel assembly with mixing vanes, simulations

were conducted with the commercial CFD software, ANSYS CFX R.14. The predicted results were compared with the measured data from the MATiS-H test facility. Through these comparisons, it was concluded that although there were locally differences between the prediction and the measurement, ANSYS CFX R.14 could qualitatively predict the time averaged vortical flow inside fuel assembly with mixing vanes. Additionally either absolute helicity or *Q*-criterion could efficiently identify vortex core region in the subchannel. Vortical flow distributions inside fuel assembly were significantly different, depending on the arrangement pattern of the mixing vane.

ACKNOWLEDGMENTS

REFERENCES

1. S.-K. CHANG, S. KIM, C.-H. SONG, "Turbulent Mixing in a Rod Bundle with Vaned Spacer Grids: OECD/NEA–KAERI CFD Benchmark Exercise Test," *Nuclear Engineering and Design*, 279, pp.19 (2014).
2. *ANSYS CFX-Solver Modeling Guide*, ANSYS Inc. (2011).
3. G.H. LEE, A.J. CHEONG, "Numerical Analysis of Flow Distribution Inside a Fuel Assembly with Split-Type Mixing Vanes," *Trans. Korean Soc. Mech. Eng. B (in Korean)*, 40, 329 (2016).
4. G.H. LEE, A.D SHIN, A.J. CHEONG, "Numerical Analysis for Flow Distribution inside a Fuel Assembly with Swirl-type Mixing Vanes," *Korean Journal of Air-Conditioning and Refrigeration Engineering (in Korean)*, 28, 186 (2016).
5. B.L. SMITH, C.H. SONG, S.K. CHANG, J.R. LEE, J.W. KIM, "Report of the OECD/NEA KAERI Rod Bundle CFD Benchmark Exercise," NEA/CSNI/R(2013), 5 (2013).